

# Molecular Dynamics Simulation of the Low-Temperature Partial Oxidation of CH<sub>4</sub>

Alister J. Page\* and Behdad Moghtaderi

Priority Research Centre for Energy, Discipline of Chemical Engineering, Faculty of Engineering and Built Environment, The University of Newcastle, University Drive, Callaghan, NSW 2308, Australia

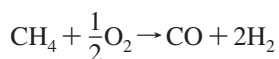
Received: October 29, 2008; Revised Manuscript Received: December 10, 2008

Low-temperature partial oxidation of methane was investigated using reactive molecular dynamics (MD) and quantum mechanical (QM) methods. In particular, the ReaxFF hydrocarbon force field [Chenoweth, K.; et al. *J. Phys. Chem. A* 2008, 112, 1040] was employed to simulate a [20 CH<sub>4</sub> + 10 O<sub>2</sub>] model system at 500 °C. The chemical mechanism of the partial oxidation of methane was proposed on the basis of analysis of the computed trajectory of this model system. The partial oxidation of methane was observed to be initiated by the abstraction of hydrogen from CH<sub>4</sub> by O<sub>2</sub> and the atomization of CH<sub>4</sub> itself. Subsequent radical recombination between hydrogen atoms and the dehydrogenation of CH<sub>4</sub> were the primary pathways by which H<sub>2</sub> was formed. In agreement with current models of low-temperature combustion, radicals including H<sub>3</sub>C–OO and H<sub>2</sub>C–OO were also observed during the MD simulation. The observed reaction mechanism was subsequently analyzed using QM methods. For instance, structural features of prominent radical species observed during the MD simulation were analyzed using density functional theory (DFT) and coupled-cluster (CCSD(T)) methods. Enthalpies of reaction of all observed chemical processes were calculated using DFT and the W1 composite method. Where possible, comparisons with experimental data were made.

## Introduction

Hydrogen is thought to be a crucial component of sustainable energy scenarios in the future.<sup>1</sup> There are several reasons why this is the case. Most importantly, hydrogen is a clean fuel (oxidation yields water as the only chemical product) and exhibits a relatively large energy density (ca. 120–140 MJ kg<sup>-1</sup>). The consumption of hydrogen in the production of heat/power is also ideally suited to fuel cell technology. Despite these desirable qualities, pure hydrogen does not occur naturally on earth.<sup>2</sup> The success of using hydrogen in the context of sustainable energy production therefore depends entirely on its safe and efficient manufacture from other, primary fuel sources.

Myriad alternatives for the generation of hydrogen have been proposed to date.<sup>3–7</sup> Increasingly, however, the generation of hydrogen from the partial oxidation of methane (POM) has been considered to be an attractive option. This reaction,



although only slightly exothermic ( $\Delta_r H^\circ(298.15 \text{ K}) = -36 \text{ kJ mol}^{-1}$ ),<sup>8</sup> is extremely fast, particularly at high temperatures.<sup>9</sup> In addition, methane is readily available in many parts of the world. This chemical process is also adaptable to microscale fuel cells, making it suitable for mobile/onboard applications.<sup>10</sup> For example, our group<sup>11,12</sup> recently implemented hydrogen generation via POM in a microscale reactor.

There are a number of reviews available concerning various aspects of both noncatalytic and catalytic POM.<sup>8,13–15</sup> Most recently, Enger et al.<sup>9</sup> reviewed the reaction mechanisms associated with transition-metal-catalyzed POM. The first investigations of catalytic POM were performed by Liander,<sup>16</sup> Padovani and Franchetti,<sup>17</sup> and Prettre et al.<sup>18</sup> These investigations demonstrated that higher temperatures (i.e., greater than

850 °C) promote both methane conversion and CO/H<sub>2</sub> selectivity. Noncatalytic POM at temperatures greater than ca. 1000 °C is now a commercially viable technology.<sup>13</sup> York et al.<sup>8</sup> reported that high pressure impedes both methane conversion and product selectivity. These dependencies on both temperature and pressure of noncatalytic and catalytic POM were also recently reproduced on the microscale.<sup>12</sup> Despite the extent of the literature concerning the reaction mechanisms and kinetics of POM, no investigation has reported atomistic information regarding the initial or fundamental chemical events responsible for the conversion of methane at 500 °C. Such low temperature systems are particularly attractive from an energy efficiency perspective. However, several quantum mechanical (QM) investigations of catalytic POM reaction mechanisms have been reported (see ref 9 and references therein). To the best of our knowledge, no reported investigations have addressed the fundamental chemical processes of the POM using atomistic molecular dynamics (MD).

Although correlated QM methods increasingly provide reliable structural, thermochemical, and kinetic data for many atomic and molecular species, their computational expense limits their practical application to only the simplest reactive systems. Conversely, traditional MD force fields allow for the simulation of large-scale properties (i.e., in excess of millions of atoms) and are applicable to a wide range of species. Nevertheless, MD methods generally fail to describe the processes of bond breaking and bond formation. The force field of Brenner<sup>19</sup> developed for hydrocarbons is an exception, in that it allows chemical bonds to be broken. The approach of Brenner is an extension of the bond order/bond distance relationship introduced by Tersoff.<sup>20</sup> In this case, the connectivity of every atom in the system of interest is determined at each iteration and is a function of bond order. This allows the connectivity of the system to vary with time. However, the Brenner force field lacks an explicit description of Coulombic and van der Waals interactions. Dissociative potential energy surfaces predicted

\* To whom correspondence should be addressed. E-mail: alister.page@newcastle.edu.au.

using the Brenner force field are therefore often lacking in a quantitative sense. Similar “reactive” force fields include the bond energy bond order method of Johnston and co-workers<sup>21,22</sup> and the VALBOND method of Landis and co-workers.<sup>23–25</sup> The former of these force fields is based on the relationship between bond order and bond length proposed by Pauling.<sup>26</sup>

A more recent approach is that of van Duin and co-workers, who investigated hydrocarbons,<sup>27,28</sup> nitramines,<sup>29</sup> oxides of various main group metals,<sup>30,31</sup> carbon–silicon polymers,<sup>32</sup> and transition-metal catalysis<sup>33–35</sup> using their ReaxFF force field. This force field explicitly includes descriptions of Coulombic and van der Waals interactions and also describes the valence/torsion angles, bond conjugation, and polarization effects at each iteration of the MD simulation. These structural phenomena are therefore included in the description of bond formation and bond breaking. At small internuclear distances, the repulsive force experienced between atoms is controlled by shielding functions. The parameters defining the ReaxFF force field are tuned against an extensive set of structural and energetic data that were calculated using density functional theory (DFT). Chenoweth et al.<sup>28</sup> recently extended the ReaxFF hydrocarbon force field QM training set to include chemical reactivity and transition-state data typically observed during hydrocarbon oxidation. Hence, a more complete chemical description of low-temperature POM would be attained using this method.

We wish to present here a theoretical investigation of low-temperature POM. The ReaxFF hydrocarbon force field reported by van Duin et al.<sup>27,28</sup> will be used to simulate the reaction between CH<sub>4</sub> and O<sub>2</sub> at 500 °C. The low-temperature POM was modeled using a model system of CH<sub>4</sub> and O<sub>2</sub> molecules in the stoichiometric ratio 2:1. The mechanism observed from analysis of the computed trajectory of the system will subsequently be discussed. Structural and energetic features of this mechanism will then be analyzed in greater detail. First, the equilibrium structures of prominent radical species observed during the simulation will be investigated using QM methods. Enthalpies of several reactions observed in the MD simulation will then be reported using QM methods. It is hoped that the analysis presented in this work will furnish a more complete atomistic understanding of the fundamental processes observed in low-temperature oxidative processes of simple hydrocarbons.

## Computational Methods

**Molecular Dynamics Simulations.** A periodic system of 20 CH<sub>4</sub> and 10 O<sub>2</sub> molecules was simulated using the ReaxFF force field.<sup>27,28</sup> The dimensions and density of the system were 20 × 15 × 15 Å<sup>3</sup> and 0.40 kg dm<sup>-3</sup>, respectively. Throughout the MD simulation, the number of atoms and the volume/temperature of the periodic system were held constant (conditions denoted by NVT). The system temperature was maintained via a Berendsen thermostat<sup>36</sup> with a 2.5-fs damping constant. The system was initially equilibrated at 500 °C (773.15 K) for 100 ps using NVT-MD with a 0.1-fs time step. Chenoweth et al.<sup>28</sup> employed this time step for high-temperature (2500 K) MD hydrocarbon oxidation and noted that this time step allows for a consistent description of the charges and bond orders in the system (both of which can change at each time step), and therefore facilitated a consistent description of chemical processes. An NVT-MD time step of 0.1 fs is anticipated to suffice in this work. Fluctuations in the kinetic energy and dynamics properties of individual particles in an MD simulation are not significantly altered using damping constants ca. 1–2 orders of magnitude greater than Δ*t*, such as that employed here. Nevertheless, fluctuations in the total energy of the system are,

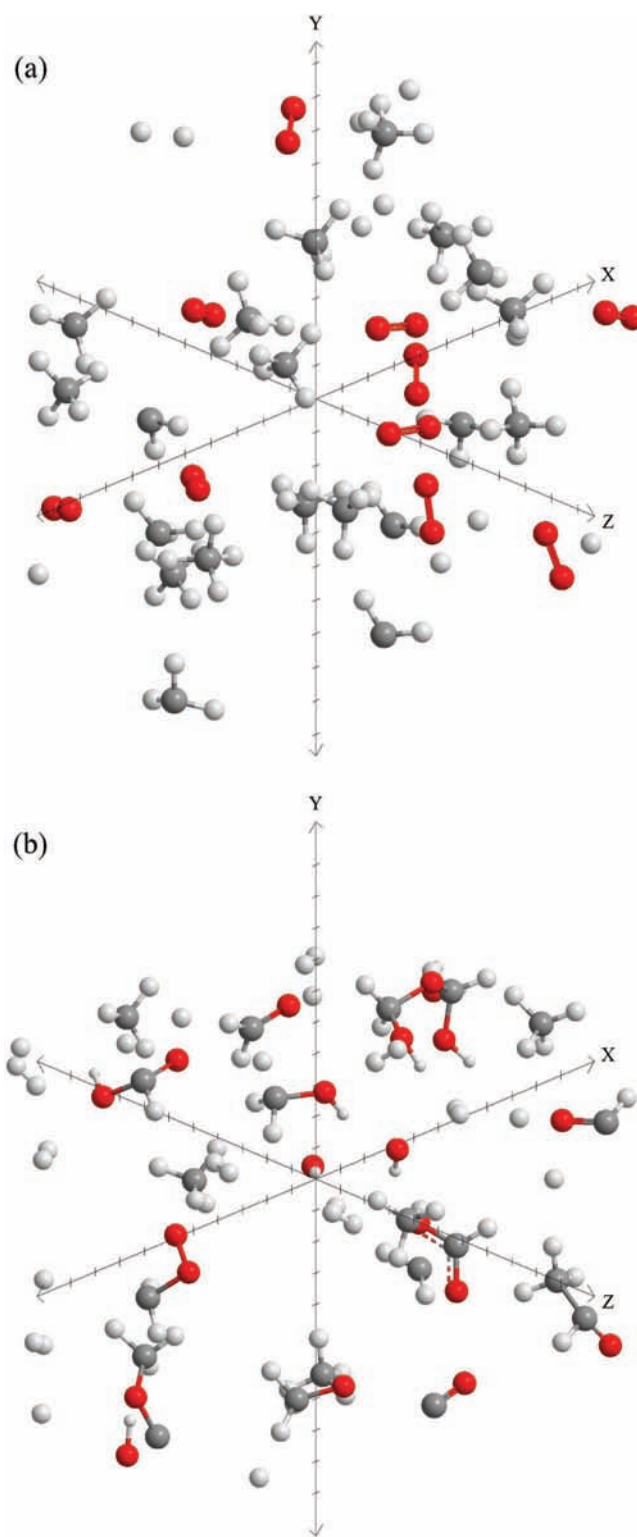


**Figure 1.** [20 CH<sub>4</sub> + 10 O<sub>2</sub>] system after (a) 100-ps NVT-MD equilibration at 773.15 K and (b) 3000-ps NVT-MD reaction at 773.15 K.

to a large extent, artifacts of MD approaches and are associated with smaller temperature damping constants (i.e., <0.01 ps).<sup>36</sup> Reactions between O–C and O–H were prevented during the 100-ps equilibration period by eliminating the bond parameters describing these interactions from the force field. The final equilibrated system geometry is shown in Figure 1a. The equilibrated system geometry was then employed in a 500 °C (773.15 K) NVT-MD simulation that employed a simulation

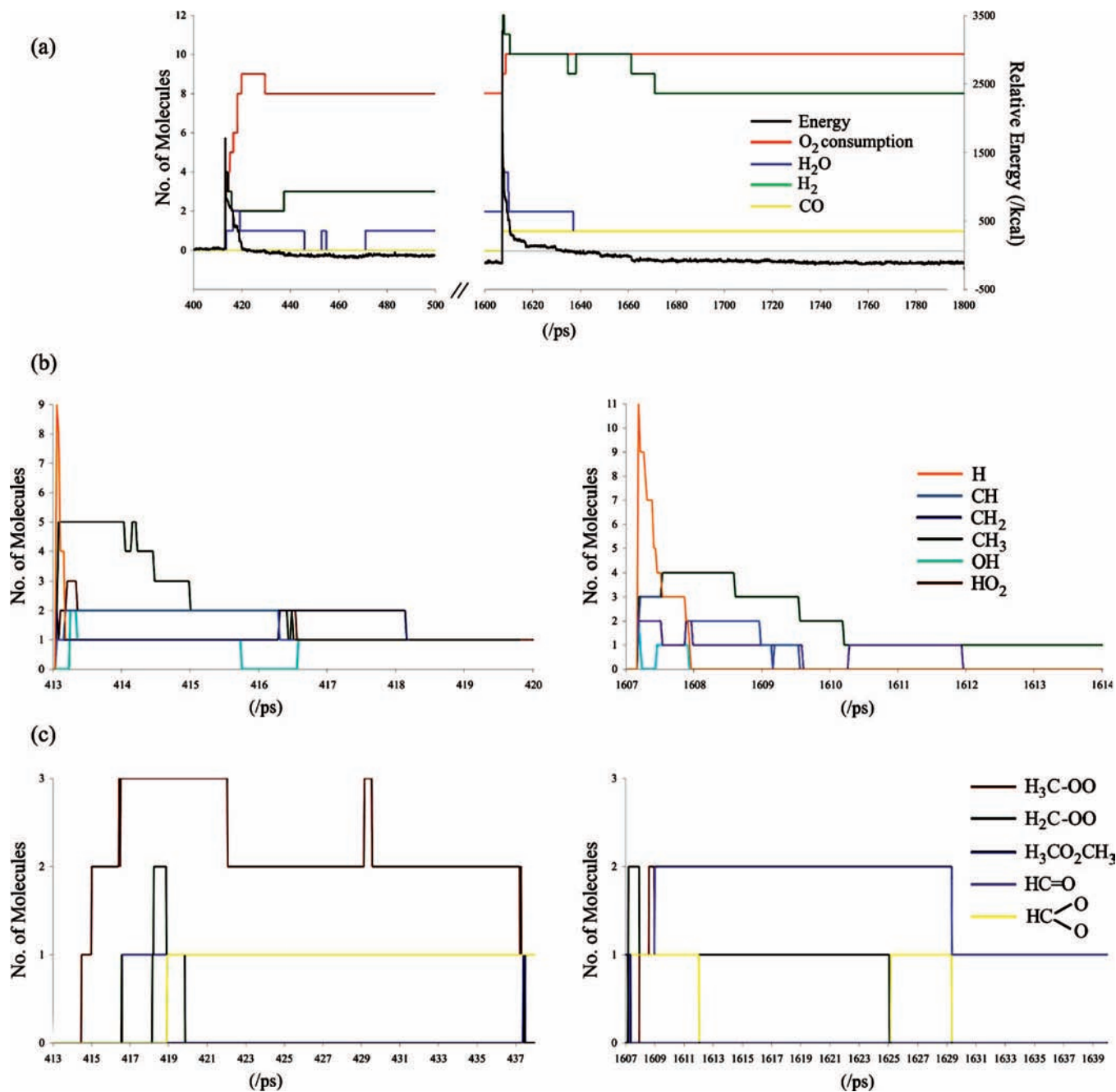


**Figure 2.** Molecular composition and total energy of the NVT-MD simulation as a function of time. (a) Major products. (b) Initial radical species. (c) Minor products.

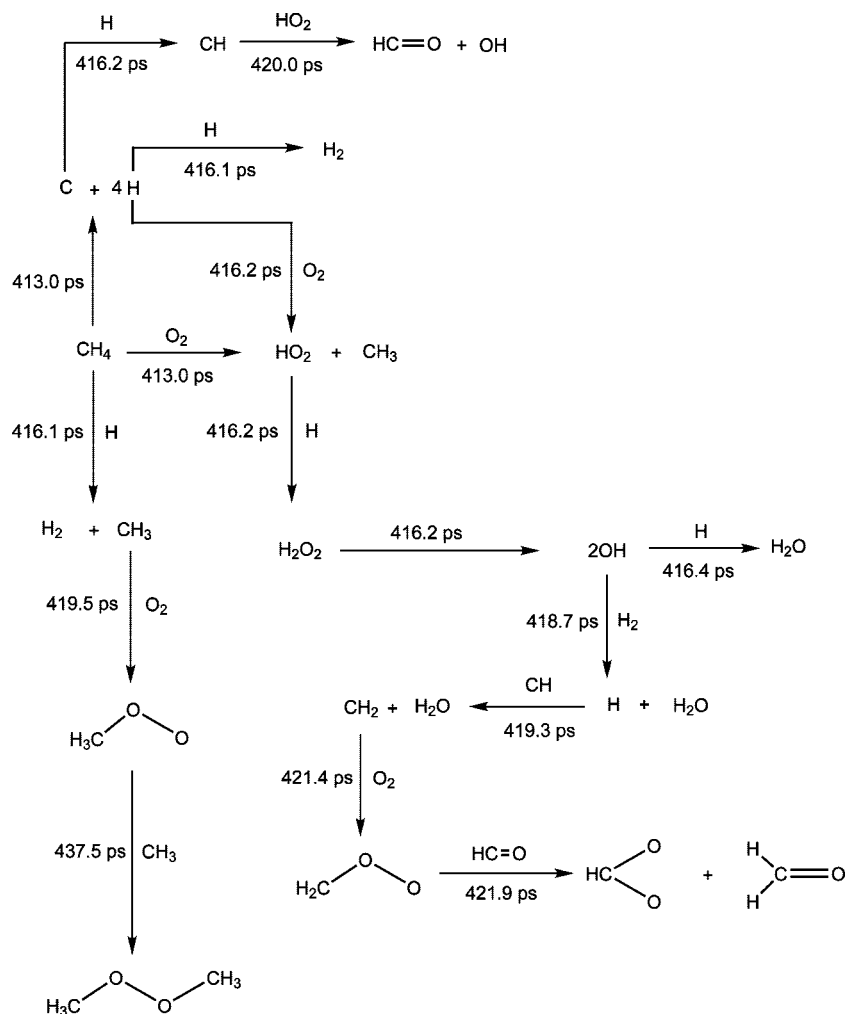
time step of 0.1 fs. The latter NVT-MD simulation was continued for 3000 ps. The final system composition is shown in Figure 1b. (It is noted here that apparent molecular fragmentation of species in the vicinity of the boundaries of the periodic box (observed in Figure 1) is unavoidable.) The pressure employed throughout these NVT-MD simulations was 101.3 kPa.

**Quantum Mechanical Calculations.** Equilibrium structural parameters (including bond lengths ( $R_e$ ) and bond angles ( $\theta_e$ )) of prominent radical species observed during the initiation of the POM were calculated using the B3LYP hybrid DFT functional<sup>37,38</sup> and coupled-cluster with singles, doubles, and perturbative triples (CCSD(T)). Comparison with the latter method allows us to gauge the effects of dynamical electron correlation more accurately. The 6-311G\*\* one-electron basis set<sup>39</sup> was used in both DFT and CCSD(T) calculations. This

basis set was also used in the development of the hydrocarbon ReaxFF force field parameters. These parameters were optimized so as to reproduce the energy corresponding to the lowest energy spin state of each molecule.<sup>28</sup> In order that consistency with the results of the ReaxFF simulation was attained, it was ensured that all DFT and CCSD(T) energies/structures corresponded to those of the lowest energy spin states. For both B3LYP/6-311G\*\* and CCSD(T)/6-311G\*\* methods, a spin-restricted Hartree-Fock determinant was employed as the reference function for all open-shell species. Both the B3LYP/6-311G\*\* and CCSD(T)/6-311G\*\* methods employed a frozen core consisting of the C and O 1s atomic orbitals.

The thermochemistry of several reactions observed during the NVT-MD simulation was also investigated quantum mechanically. Enthalpies of reaction at 298.15 K ( $\Delta_r H^\circ(298.15 \text{ K})$ ) were calculated using the ReaxFF force field and B3LYP/

## SCHEME 1: Initiation Reaction Mechanism Observed during the NVT-MD Simulation



6–311G\*\*. All DFT frequencies were scaled by a factor of 0.9826<sup>40</sup> to account for anharmonic effects. Where possible, these calculated  $\Delta_r H^\circ(298.15\text{ K})$  values were compared with experimental data. The Weizmann-1 (W1) thermochemical composite method,<sup>41</sup> as implemented in the Gaussian03 program,<sup>42</sup> was also employed to provide a comparable  $\Delta_r H^\circ(298.15\text{ K})$  value for those reactions for which no experimental data are available.

All DFT and CCSD(T) calculations were performed using the Gaussian03<sup>42</sup> and AcesII<sup>43</sup> programs, respectively.

## Results and Discussion

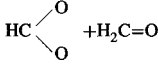
### NVT-MD Simulation of the Partial Oxidation of CH<sub>4</sub>.

Figure 2 summarizes the molecular composition and total energy of the [20 CH<sub>4</sub> + 10 O<sub>2</sub>] NVT-MD simulation as a function of time. In particular, Figure 2a shows the total energy of the system and the abundance of expected products (viz. H<sub>2</sub>, H<sub>2</sub>O, CO), Figure 2b shows the abundance of prominent radical species (viz. OH, HO<sub>2</sub>, CH<sub>3</sub>, CH<sub>2</sub>, CH, and H), and Figure 2c shows the abundance of other persistent species observed during the simulation. No chemical activity was observed before 413 ps. Similarly, the final chemical composition of the system was attained at 1800 ps. The NVT-MD simulation was continued for a further 1200 ps, during which very little chemical activity was observed due to the depletion of O<sub>2</sub>. Those reactions that were observed were addition processes involving several larger radical species present in the simulation and were not deemed

pertinent in the present context. The exothermicity of the overall reaction during the 413–438- and 1607–1640-ps time periods is evident in Figure 2a. It is also evident from Figure 2b,c that similar populations of various radical species were observed during these time periods. It was therefore concluded that the POM observed here proceeded by very similar, if not identical, mechanisms. The chemical reaction mechanism observed during the 413–438-ps period of the NVT-MD simulation was reported in Scheme 1. All steps reported in this reaction mechanism were observed directly during analysis of the computed MD trajectory of the model system.

The oxidation of CH<sub>4</sub> was initiated by the abstraction of hydrogen from CH<sub>4</sub> by O<sub>2</sub>, forming HO<sub>2</sub> and CH<sub>3</sub>. This is consistent with established mechanisms present in the literature.<sup>28,44</sup> However, the atomization of CH<sub>4</sub> was observed to be simultaneous with this initial hydroperoxy radical formation at ca. 413 ps. The atomization of CH<sub>4</sub> was also observed at ca. 1607 ps. Partial atomizations of CH<sub>4</sub> (i.e., reactions such as [CH<sub>4</sub> → CH<sub>3</sub> + H] and [CH<sub>4</sub> → CH<sub>2</sub> + 2H]) were also observed at ca. 1607 ps. The increases in the total energy of the system at ca. 413 and 1607 ps are concomitant with  $\Delta_r H^\circ(298.15\text{ K})$  data concerning these separate atomization processes (Table 1), as are the number of H radicals present in the system. Chenoweth et al.<sup>28</sup> calculated the barriers for the [CH<sub>4</sub> + O<sub>2</sub> → CH<sub>3</sub> + HO<sub>2</sub>] and [CH<sub>3</sub> + HO<sub>2</sub> → CH<sub>4</sub> + O<sub>2</sub>] reactions to be ca. 50 and 8 kcal mol<sup>-1</sup>, respectively. However, the reaction [CH<sub>3</sub> + O<sub>2</sub> → H<sub>3</sub>C–OO] is exothermic and barrierless.<sup>45</sup> The re-

**TABLE 1: Comparison of Experimental and Theoretical Reaction Enthalpies (kcal mol<sup>-1</sup>) for Reactions Observed during the ReaxFF Simulation**

Reaction	$\Delta_r H^\circ(298.15 \text{ K})$			
	REAXFF	DFT	W1	Expt.
CH <sub>4</sub> → C + 4H	463.3	400.2	393.8	395.7 <sup>1</sup>
C + H → CH	-118.7	-81.3	-79.9	-81.39 <sup>1</sup>
CH + H → CH <sub>2</sub>	-115.3	-101.9	-100.2	-101.8 <sup>1</sup>
CH <sub>4</sub> + H → H <sub>2</sub> + CH <sub>3</sub>	1.4	2.2	0.6	0.6 <sup>1</sup>
CH <sub>4</sub> + O <sub>2</sub> → HO <sub>2</sub> + CH <sub>3</sub>	41.2	57.3	56.3	53.2 <sup>1</sup>
CH <sub>3</sub> + O <sub>2</sub> → H <sub>3</sub> C-OO	-48.1	-29.7	-31.2	-30.9 <sup>2</sup>
CH <sub>2</sub> + O <sub>2</sub> → H <sub>2</sub> C-OO	-59.4	-71.0	-74.0	
CH + HO <sub>2</sub> → HC=O + OH	-118.0	-124.2	-126.8	-122.8 <sup>1</sup>
O <sub>2</sub> + H → HO <sub>2</sub>	-69.8	-48.2	-47.6	-51.6 <sup>1</sup>
O <sub>2</sub> + C → CO + O	-150.7	-132.7	-138.7	-139.8 <sup>1</sup>
HO <sub>2</sub> + H → H <sub>2</sub> O <sub>2</sub>	-98.7	-81.5	-86.6	-85.1 <sup>1</sup>
H <sub>2</sub> O <sub>2</sub> → 2OH	45.2	47.5	50.2	51.17 <sup>1</sup>
OH + H → H <sub>2</sub> O	-114.2	-113.4	-118.2	-119.22 <sup>1</sup>
OH + H <sub>2</sub> → H <sub>2</sub> O + H	-4.7	-10.1	-15.0	-15.01 <sup>1</sup>
H <sub>3</sub> C-OO + CH <sub>3</sub> → H <sub>3</sub> C-OO-CH <sub>3</sub>	-70.7	-60.2	-64.5	
H <sub>2</sub> C-OO + HC=O →				
	-128.9	-96.2	-94.9	

<sup>1</sup> See ref 58. <sup>2</sup> See ref 60.

formation of CH<sub>4</sub> and O<sub>2</sub> in the NVT-MD simulation was therefore not observed via this pathway. The formation of the methylperoxy radical was observed soon after initiation at 419.5 ps. This radical species was present at various concentrations for the remainder of the NVT-MD simulation, as is evident from Figure 2c. It has been noted in a number of investigations (see ref 45 and references therein) that at atmospheric pressure the H<sub>3</sub>C-OO radical is the main product of the [CH<sub>3</sub> + O<sub>2</sub>] reaction at temperatures lower than 1000 K. At higher temperatures, however, this reaction results in association giving [H<sub>2</sub>C-O + OH] (1000–2000 K) and [H<sub>3</sub>C-O + O] (>2000 K). Petersen and co-workers<sup>46,47</sup> established the importance of radicals such as H<sub>3</sub>C-OO and H<sub>3</sub>C-O with respect to the kinetics of POM at higher temperature and pressure. The latter radical is formed from the reaction between [H<sub>3</sub>C-OO + CH<sub>3</sub>] at 1100 K and 10 MPa.<sup>48</sup> The hydrogenated form of this radical (H<sub>3</sub>C-OOH) was not observed, although its presence has been established in higher-temperature NVT-MD simulations of methane oxidation.<sup>28</sup> Nevertheless, methanol and the methoxy radical were observed at ca. 1608 and 1607 ps, respectively. The H<sub>3</sub>C-OO radical observed corresponds to a local minimum on the <sup>2</sup>A'' potential energy surface.<sup>45</sup> The observed structure of the H<sub>3</sub>C-OO radical will be discussed at greater length below. Reaction between the methyl and methylperoxy radicals was also observed at 437.5 ps, producing dimethyl peroxide, H<sub>3</sub>C-OO-CH<sub>3</sub>. This reaction was exothermic and corresponded to a  $\Delta_r H^\circ(298.15 \text{ K})$  of ca. -60 kcal mol<sup>-1</sup>.

The formation of H<sub>2</sub>O<sub>2</sub> (from the addition of H and HO<sub>2</sub>) was observed in the NVT-MD simulation at 416.2 ps. This addition was competitive with the formation of HO<sub>2</sub> itself, because of the comparable concentrations of H, O<sub>2</sub>, and HO<sub>2</sub> during this period. This is consistent with the conclusion of Chenoweth et al.,<sup>28</sup> who proposed that the presence of HO<sub>2</sub> radicals is determined by the relative levels of H, OH, and O<sub>2</sub> in the system. Interestingly, this consistency occurs despite a large temperature difference (ca. 1800 K). The H<sub>2</sub>O<sub>2</sub> radical species dissociated quickly, forming two hydroxyl radicals.

Water was subsequently formed via two different reactions. First, addition of H to OH at 416.4 ps resulted in the formation of H<sub>2</sub>O. The abstraction of hydrogen from H<sub>2</sub> also gave H<sub>2</sub>O according to [OH + H<sub>2</sub> → H<sub>2</sub>O + H]. Both of these processes are exothermic; however, the former addition process corresponded to a  $\Delta_r H^\circ(298.15 \text{ K})$  value ca. 10 times that of the latter abstraction.

Following the atomization of CH<sub>4</sub>, the [C + H → CH] and [CH + H → CH<sub>2</sub>] recombination reactions were observed at 416.2 and 419.3 ps, respectively. This was anticipated, given the increased concentrations of free C and H during these periods of the NVT-MD simulation. These recombination reactions were also observed at 1610.3 and 1608.3 ps. However, no further hydrogenation of the methylene radical was observed. This was attributed to the presence of the competing [H + H → H<sub>2</sub>] radical recombination reaction. The latter process was observed to be the primary mechanism by which H<sub>2</sub> was formed during the NVT-MD simulation and was initially observed at 416.1 ps. From Figure 2, it is evident that the sharp decrease in H concentration at 413–414 and 1607–1608 ps is accompanied by increasing concentrations of H<sub>2</sub>, CH, and CH<sub>2</sub>. The methyldyne radical was relatively short-lived and was not observed in the simulation after 1609 ps. The majority of H<sub>2</sub> present at the end of the NVT-MD simulation was formed within the first 4 ps of both reaction initiations, as observed in Figure 2a. However, H<sub>2</sub> formation was observed as late as ca. 437 and 2171 ps. A second, less prominent process resulting in the formation of H<sub>2</sub> was also observed, viz. the abstraction of H by CH<sub>4</sub>, resulting in CH<sub>3</sub>. This process was observed immediately after initiation at 416.1 ps and is slightly endothermic ( $\Delta_r H^\circ(298.15 \text{ K}) \approx 0.6 \text{ kcal mol}^{-1}$ ; see Table 1).

The methyldyne and hydroperoxyl radicals also reacted, yielding the formyl (HC=O) and hydroxyl radicals. This process, observed at 420.0 ps, corresponded to a  $\Delta_r H^\circ(298.15 \text{ K})$  value of ca. -123 kcal mol<sup>-1</sup>. Similarly, the methylene radical combined with O<sub>2</sub>, giving the Criegee intermediate radical, H<sub>2</sub>C-OO. This diradical has been ascribed fundamental roles in processes such as combustion and atmospheric photochemical processes.<sup>49,50</sup> Nevertheless, it was only observed for the first time very recently in mass-spectral experiments.<sup>49</sup> It has also been the subject of a number of ab initio investigations (see refs 51 and 52 and references therein), and debate over the electronic structure of this species is ongoing. In agreement with available theoretical data,<sup>51,52</sup> the [CH<sub>2</sub> + O<sub>2</sub>] reaction observed in the NVT-MD simulation of the present work was exothermic and corresponded to a  $\Delta_r H^\circ(298.15 \text{ K})$  of ca. -60 kcal mol<sup>-1</sup>. The H<sub>2</sub>C-OO structure observed here corresponds to a stable intermediate structure on the <sup>1</sup>A' potential energy surface. According to the ab initio data of both Chen et al.<sup>51</sup> and Fang and Fu,<sup>52</sup> this diradical ultimately dissociates, producing CO, CO<sub>2</sub>, and H<sub>2</sub>. The reaction paths proposed by Alvarez and Moore<sup>53</sup> also yield CO, H<sub>2</sub>O, CO<sub>2</sub>, and H<sub>2</sub> from the decomposition of a formic acid intermediate. No dissociation processes of this type were observed in the present work, since reaction between the HC=O and H<sub>2</sub>C-OO radicals occurred ca. 0.5 ps following the formation of the latter species. This reaction resulted in a planar HCO<sub>2</sub> radical (Figure 3) and formaldehyde. The former of these species has been investigated previously using DFT in the context of the [CH + O<sub>2</sub>] reaction.<sup>54</sup> The planar HCO<sub>2</sub> radical observed has been identified as the <sup>2</sup>A<sub>1</sub> stable intermediate structure investigated by Huang et al.<sup>54</sup> According to their B3LYP/6-311++G(d,p) potential energy surface, the HCO<sub>2</sub> radical dissociates, giving [CO<sub>2</sub> + H] and [CO + OH]. These respective exothermic and endothermic processes were

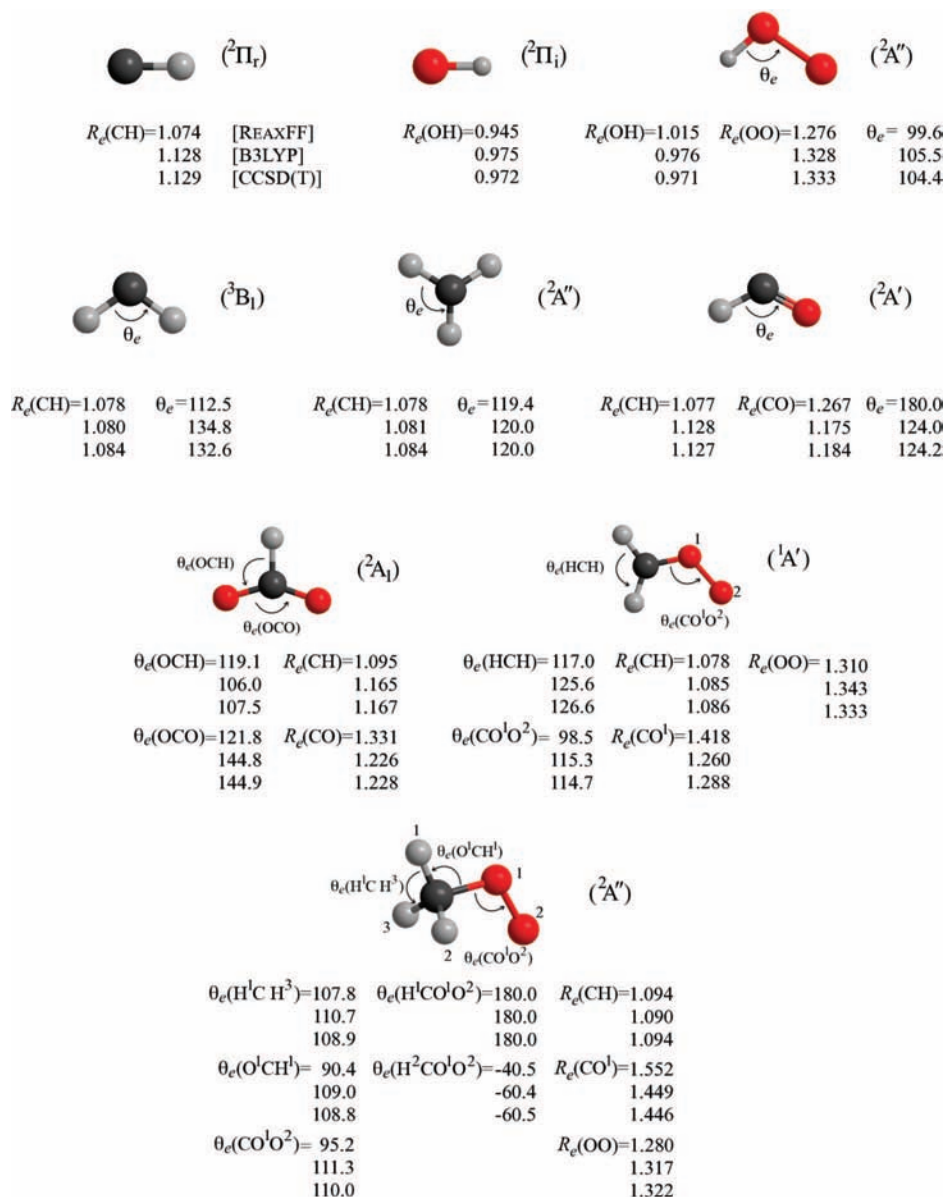


**Figure 3.** Comparison of the equilibrium structures of prominent radical species observed during the ReaxFF simulation, using ReaxFF, B3LYP/6-311G\*\*, and CCSD(T)/6-311G\*\*. Bond lengths and angles are given in angstroms and degrees, respectively.

not observed in the present work. However, it is anticipated that the production of  $\text{CO}_2$ , H, CO, and OH from the decomposition of  $\text{HCO}_2$  would be observed on longer time scales than that employed here. Nevertheless, the production of CO via  $[\text{C} + \text{O}_2 \rightarrow \text{CO} + \text{O}]$  was observed at 1607.3 ps. This process exhibits a  $\Delta_r H^\circ(298.15 \text{ K})$  value of ca.  $-140 \text{ kcal mol}^{-1}$ , as is evident from Table 1.

Five  $\text{CH}_4$  molecules remained in the NVT-MD simulation following 1800 ps of simulation time. This represents a 75% conversion of  $\text{CH}_4$ . After 1800 ps, all  $\text{O}_2$  molecules present at the beginning of the simulation had been consumed. Further oxidation involving  $\text{O}_2$  was therefore impossible. At a temperature of 500 °C, a pressure of 101.3 kPa, and a Reynolds number of 100, the total conversion of  $\text{CH}_4$  determined in microreactor experiments was  $16 \pm 4\%$ .<sup>12</sup> Thus, the conversion of  $\text{CH}_4$  predicted in this work is significantly larger than that derived from experimental data. This comparison is less than ideal, however, since the extent of the simulated POM is expected to decrease at larger (i.e., micro) scales. Similarly, a comparison between QM/experimental kinetics and that derived from this

NVT-MD simulation is limited because of the “ideal” nature of the model system employed. For instance, current data<sup>44</sup> indicate that at 500 °C the  $[\text{CH}_4 + \text{O}_2 \rightarrow \text{CH}_3 + \text{HO}_2]$  abstraction reaction possesses a rate coefficient of ca.  $6.73 \times 10^{-26} \text{ cm}^3 \text{ molecule}^{-1} \text{ s}^{-1}$ . From this rate coefficient, it is inferred that the entire POM process would occur on time scales much greater than that predicted here (ca. 3000 ps). However, at larger scales the influence of fluidic characteristics (transport properties, diffusion, etc.) and the subsequent effect on chemical reactivity must be taken into account if a realistic simulation of this chemical reaction and its kinetics is to be attained.

#### Quantum Mechanical Analysis of the ReaxFF Mechanism.

The presence of several radical species observed in the ReaxFF simulation discussed previously (Scheme 1) necessitates further analysis of their respective equilibrium structures. It is therefore appropriate to investigate both the equilibrium structures and thermochemistry of these species using the QM methods outlined previously.

**Equilibrium Structures of Radical Species.** Equilibrium structures of prominent radical species ( $(^2\Pi_r)\text{CH}$ ,  $(^2\Pi_i)\text{OH}$ ,

(<sup>2</sup>A'')HO<sub>2</sub>, (<sup>3</sup>B<sub>1</sub>)CH<sub>2</sub>, (<sup>2</sup>A'')CH<sub>3</sub>, (<sup>2</sup>A')HC=O, (<sup>2</sup>A<sub>1</sub>)HCO<sub>2</sub>, (<sup>1</sup>A')H<sub>2</sub>C=OO, and (<sup>2</sup>A'')H<sub>3</sub>C=OO) were determined using B3LYP/6-311G\*\* and CCSD(T)/6-311G\*\* methods. In all cases, vibrational frequencies of the equilibrated structures were calculated to ensure that the structure corresponded to a local minimum on the respective potential energy surface. These structures are given in Figure 3.

The B3LYP/6-311G\*\* and CCSD(T)/6-311G\*\* equilibrium structures for the smaller radical species presented in Figure 3 were in very good agreement, as anticipated. For example,  $R_e(\text{C-H})$  for (<sup>2</sup>Π<sub>1</sub>)CH, (<sup>3</sup>B<sub>1</sub>)CH<sub>2</sub>, and (<sup>2</sup>A'')CH<sub>3</sub> differed by 0.001, 0.004, and 0.003 Å, respectively. The equilibrium C-H bond length of the formyl radical differed by ca. 0.001 Å using these methods. Similarly,  $R_e(\text{O-H})$  for (<sup>2</sup>Π<sub>1</sub>)OH and (<sup>2</sup>A'')HO<sub>2</sub> differed by at most 0.003 and 0.005 Å, respectively. With respect to bond angles, DFT and CCSD(T)  $\theta_e$  values for (<sup>2</sup>A'')HO<sub>2</sub> and (<sup>3</sup>B<sub>1</sub>)CH<sub>2</sub> agreed to within 1.1 and 2.2°, respectively, while  $\theta_e$  for (<sup>2</sup>A'')CH<sub>3</sub> was in exact agreement. With respect to the <sup>2</sup>A<sub>1</sub> state of HCO<sub>2</sub>, B3LYP/6-311G\*\* and CCSD(T)/6-311G\*\* yielded  $R_e(\text{C-H})$  and  $R_e(\text{C-O})$  values that differed by 0.002 Å. The equilibrium OCH and OCO bond angles for this species were also consistent using these methods. Explicitly, these bond angles differed by 1.5 and 0.1°, respectively.

Equilibrium structures calculated using the ReaxFF force field were also in generally good agreement with those using CCSD(T)/6-311G\*\*. For instance,  $R_e(\text{C-H})$  values for the methylene and methyl radicals were 0.006 Å smaller than that obtained using the latter method. Similarly,  $R_e(\text{O-H})$  for (<sup>2</sup>Π<sub>1</sub>)OH and (<sup>2</sup>A'')HO<sub>2</sub> differed from the CCSD(T)/6-311G\*\* values by -0.027 and 0.044 Å, respectively. The  $\theta_e$  values of (<sup>2</sup>A'')HO<sub>2</sub>, (<sup>3</sup>B<sub>1</sub>)CH<sub>2</sub>, and (<sup>2</sup>A'')CH<sub>3</sub> calculated using ReaxFF differed from the CCSD(T)/6-311G\*\* values by -4.8, -20.1, and 0.6°, respectively.

The structure of the Criegee intermediate radical (H<sub>2</sub>C=OO) observed in the NVT-MD simulation was also investigated using B3LYP/6-311G\*\* and CCSD(T)/6-311G\*\*. This structure corresponds to a local minimum on the <sup>1</sup>A' potential energy surface.<sup>51,52</sup> From Figure 3, it is evident that DFT and CCSD(T) yielded consistent structural data. For example, B3LYP/6-311G\*\* and CCSD(T)/6-311G\*\*  $R_e(\text{C-H})$ ,  $R_e(\text{C-O})$ , and  $R_e(\text{O-O})$  values differed by 0.001, 0.028, and 0.010 Å, respectively. In addition,  $\theta_e(\text{HCH})$  and  $\theta_e(\text{CO}^1\text{O}^2)$  values calculated using these methods agreed to within 1.0 and 0.6°, respectively. These data were also consistent with the complete active space (CASSCF) calculations of Chen et al.<sup>51</sup> and Fang and Fu<sup>52</sup> who employed 6-311+G(3df,2dp)<sup>39,55,56</sup> and cc-pVDZ<sup>57</sup> basis sets, respectively. For example, the greatest absolute difference observed between the  $R_e(\text{C-H})$ ,  $R_e(\text{C-O})$ , and  $R_e(\text{O-O})$  values were 0.005, 0.020, and 0.025 Å, respectively. With respect to the  $\theta_e(\text{HCH})$  and  $\theta_e(\text{CO}^1\text{O}^2)$  bond angles, the absolute greatest discrepancies observed were 1.5 and 4.8°, respectively. The stable intermediate structure located on the triplet potential energy surface was also located using CCSD(T). This structure is consistent with that reported by Fang and Fu.<sup>52</sup> Compared to the structure of (<sup>1</sup>A')H<sub>2</sub>C=OO,  $R_e(\text{C-H})$ ,  $R_e(\text{C-O})$ , and  $R_e(\text{O-O})$  for (<sup>3</sup>A'')H<sub>2</sub>C=OO calculated using CCSD(T) were 1.163, 1.423, and 1.531 Å. The (<sup>3</sup>A'')H<sub>2</sub>C=OO equilibrium bond angles calculated at this level of theory were 115.5 ( $\theta_e(\text{HCO}^1)$ ), 106.4 ( $\theta_e(\text{CO}^1\text{O}^2)$ ), and -51.2° ( $\theta_e(\text{HCO}^1\text{O}^2)$ ). In addition, the higher-spin triplet equilibrium structure lay 164.97 kcal mol<sup>-1</sup> above the (<sup>1</sup>A')H<sub>2</sub>C=OO species using CCSD(T)/6-311G\*\*.

Equilibrium structures of the trans conformer of the methylperoxy radical calculated using B3LYP/6-311G\*\* and CCS-

D(T)/6-311G\*\* are given in Figure 3. This structure corresponds to a local minimum on the <sup>2</sup>A'' [CH<sub>3</sub> + O<sub>2</sub>] potential energy surface.<sup>45</sup> It was observed that these methods yielded equilibrium structures that were in good agreement. With respect to bond lengths,  $R_e(\text{C-H})$ ,  $R_e(\text{C-O})$ , and  $R_e(\text{O-O})$  calculated using these methods differed by 0.004, 0.003, and 0.005 Å, respectively. Similarly, the equilibrium bond angles  $\theta_e(\text{H}^1\text{CH}^3)$ ,  $\theta_e(\text{O}^1\text{CH}^1)$ , and  $\theta_e(\text{CO}^1\text{O}^2)$  differed by 1.8, 0.2, and 1.3°, respectively. This consistency was also evident in the calculated equilibrium  $\theta_e(\text{H}^2\text{CO}^1\text{O}^2)$  dihedral angles, which differed by only 0.1°. Moreover, the  $\theta_e(\text{H}^1\text{CO}^1\text{O}^2)$  dihedral angle was identical using B3LYP/6-311G\*\* and CCSD(T)/6-311G\*\*. The cis form of the methylperoxy radical was also characterized here using CCSD(T)/6-311G\*\*. This conformer (for which  $\theta_e(\text{H}^1\text{CO}^1\text{O}^2) = 0^\circ$ ) lay 1.19 kcal mol<sup>-1</sup> above the lower energy trans conformer. This is in good agreement with the B3LYP/6-311G(d,p) value of Zhu et al.,<sup>45</sup> being 0.8 kcal mol<sup>-1</sup>. The cis conformer corresponds to a first-order transition state on the <sup>2</sup>A''[CH<sub>3</sub> + O<sub>2</sub>] potential energy surface. At the CCSD(T)/6-311G\*\* level of theory, the imaginary frequency was 515.6 cm<sup>-1</sup>, compared to the B3LYP/6-311G(d, p) value of 137 cm<sup>-1</sup>.<sup>45</sup>

**Reaction Enthalpies.** Enthalpies of reaction were determined here using ReaxFF, B3LYP/6-311G\*\*, and the W1 composite method at 298.15 K. This facilitates comparison with experimental data, where available. Comparing  $\Delta_r H^\circ(298.15 \text{ K})$  data in this way will provide an indication as to the efficacy of both the predicted reaction mechanism and the overall simulation.

From Table 1, it is evident that for all reactions observed during the NVT-MD simulation,  $\Delta_r H^\circ(298.15 \text{ K})$  values calculated using ReaxFF are qualitatively consistent with experimental values and those calculated using both B3LYP/6-311G\*\* and W1. Of all the reactions observed in the NVT-MD simulation, only four are endothermic. Moreover, it is evident that these endothermic processes were observed either during or soon after the initiation of the oxidative process. This is consistent with the total energy of the system shown in Figure 2a. For example, the reaction [CH<sub>4</sub> → C + 4H] exhibited a  $\Delta_r H^\circ(298.15 \text{ K})$  value of ca. 400 kcal mol<sup>-1</sup>. The [CH<sub>4</sub> + O<sub>2</sub> → HO<sub>2</sub> + CH<sub>3</sub>] and [H<sub>2</sub>O<sub>2</sub> → 2OH] reactions both exhibited  $\Delta_r H^\circ(298.15 \text{ K})$  values of ca. 50 kcal mol<sup>-1</sup>. The [CH<sub>4</sub> + H → H<sub>2</sub> + CH<sub>3</sub>] reaction is also slightly endothermic, with  $\Delta_r H^\circ(298.15 \text{ K})$  being ca. 0.5 kcal mol<sup>-1</sup>. With respect to the latter reaction, ReaxFF, B3LYP/6-311G\*\*, and W1 gave consistent results with the experimental value of 0.6 ± 0.1 kcal mol<sup>-1</sup>.<sup>58</sup>

The hydrogenation of both C and CH are both exothermic processes. There was reasonable agreement between theoretical and experimental  $\Delta_r H^\circ(298.15 \text{ K})$  values for these reactions. For example, using ReaxFF, B3LYP/6-311G\*\*, and W1, differences from experiment of ca. -37.3, 0.0, and 1.4 kcal mol<sup>-1</sup> were observed with respect to the hydrogenation of C. For the latter hydrogenation reaction these differences were, respectively, -13.5, -0.1, and 1.6 kcal mol<sup>-1</sup>. The hydrogenation of O<sub>2</sub>, HO<sub>2</sub>, and OH were also observed to be exothermic. Moreover, there was better agreement between the methods employed here and experimental data. For example, for the reaction [O<sub>2</sub> + H → HO<sub>2</sub>], ReaxFF, B3LYP/6-311G\*\*, and W1  $\Delta_r H^\circ(298.15 \text{ K})$  values were -69.8, -48.2, and -47.6 kcal mol<sup>-1</sup>, and thus differed from experiment by -18.2, 3.4, and 4.0 kcal mol<sup>-1</sup>. Similarly, for the [HO<sub>2</sub> + H → H<sub>2</sub>O<sub>2</sub>] reaction these differences were -13.6, 3.6, and -1.5 kcal mol<sup>-1</sup>, whereas for the [OH + H → H<sub>2</sub>O] reaction they were 5.0, 5.2, and 0.4 kcal mol<sup>-1</sup>, respectively.

The addition of oxygen to the methyl and methylene radicals is an exothermic process. There is no experimental data concerning  $[\text{CH}_2 + \text{O}_2 \rightarrow \text{H}_2\text{C}-\text{OO}]$  available in the literature. However, Chen et al.<sup>51</sup> reported a  $\Delta_r H^\circ(298.15 \text{ K})$  value for this addition reaction of  $-49.1 \text{ kcal mol}^{-1}$  using CASPT2/6-311+G(3df,2p). Slagle and Gutman<sup>60</sup> reported a  $\Delta_r H^\circ(298.15 \text{ K})$  of  $-30.9 \pm 0.9 \text{ kcal mol}^{-1}$  for the  $[\text{CH}_3 + \text{O}_2 \rightarrow \text{H}_3\text{C}-\text{OO}]$  reaction from experimental data. Zhu et al.<sup>45</sup> also reported a  $\Delta_r H^\circ(298.15 \text{ K})$  value of  $-30.4 \text{ kcal mol}^{-1}$  for this latter reaction using the G2 composite method.<sup>59</sup> The theoretical data listed in Table 1 regarding the addition of  $\text{CH}_3$  and  $\text{O}_2$  are in good agreement with experiment.<sup>60</sup> For example, B3LYP/6-311G\*\* and W1 methods yield  $\Delta_r H^\circ(298.15 \text{ K})$  values that were 1.2  $\text{kcal mol}^{-1}$  greater and 0.3  $\text{kcal mol}^{-1}$  smaller, respectively. This difference for the ReaxFF  $\Delta_r H^\circ(298.15 \text{ K})$  value was larger,  $-17.2 \text{ kcal mol}^{-1}$ . Similar consistency was observed between these three theoretical methods for the formation of the Criegee intermediate. For example,  $\Delta_r H^\circ(298.15 \text{ K})$  for the reaction  $[\text{CH}_2 + \text{O}_2 \rightarrow \text{H}_2\text{C}-\text{OO}]$  calculated using ReaxFF was 11.6 and 14.6  $\text{kcal mol}^{-1}$  larger than the B3LYP/6-311G\*\* and W1 values, respectively. For the radical addition reaction  $[\text{H}_3\text{C}-\text{OO} + \text{CH}_3 \rightarrow \text{H}_3\text{C}-\text{OO}-\text{CH}_3]$ , these differences were  $-10.5$  and  $-6.2 \text{ kcal mol}^{-1}$ , respectively.

## Conclusions

Low-temperature POM was simulated using NVT-MD in conjunction with the ReaxFF hydrocarbon force field.<sup>28</sup> In particular, a  $[20 \text{ CH}_4 + 10 \text{ O}_2]$  model system was simulated at  $500 \text{ }^\circ\text{C}$ . All reactions discussed were directly observed during the analysis of the computed trajectory of this model system. The mechanism observed during the NVT-MD simulation was subsequently analyzed using QM methods. In particular, B3LYP/6-311G\*\* and CCSD(T)/6-311G\*\* methods were employed to investigate the structures of several prominent species. Enthalpies of reaction were also computed using B3LYP/6-311G\*\* and W1 methods. This comparison with QM and experimental data provided a good indication regarding the validity of the reaction mechanism observed during the NVT-MD simulation. The ReaxFF force field has therefore provided fundamental insight into the initial chemical mechanisms that feature during the partial oxidation of  $\text{CH}_4$ .

The partial oxidative process was initiated by both the abstraction of hydrogen from  $\text{CH}_4$  by  $\text{O}_2$  and the atomization of  $\text{CH}_4$  itself. Subsequent radical recombination of hydrogen was the primary mechanism by which  $\text{H}_2$  was generated. However, the abstraction of hydrogen from  $\text{CH}_4$  by hydrogen (i.e., forming  $\text{CH}_3$  and  $\text{H}_2$ ) was observed simultaneously. The final chemical composition of the system resulted from the sudden increase in the concentrations of radicals such as H, CH,  $\text{CH}_2$ ,  $\text{CH}_3$ , OH, and  $\text{HO}_2$  during the initiation of the oxidative process. Because of the high radical concentration during this period, radical recombination processes observed in the NVT-MD simulation resulted in species such as  $\text{HC}=\text{O}$ ,  $\text{HCO}_2$ , and  $\text{H}_3\text{C}-\text{OO}-\text{CH}_3$ . The methylperoxy and Criegee intermediate radicals were also observed during the NVT-MD simulation. The presence of these radicals was consistent with the conclusions of previous investigations of low-temperature combustion.<sup>45,48</sup> Stoichiometric production of  $\text{H}_2$  was not observed during the reaction; however, the percentage conversion of  $\text{CH}_4$  was significantly larger than the value derived from recent experiments.<sup>12</sup>

**Acknowledgment.** A.J.P. thanks Dr. Adri van Duin of Pennsylvania State University for the use of the ReaxFF code

and his related advice and assistance. We acknowledge computing support from the Australian Centre for Advanced Computing and Communications (AC<sup>3</sup>) and the High-Performance Computing facility of the University of Newcastle, Australia.

## References and Notes

- (1) Winter, J. C. *Int. J. Hydrogen Energy* **2004**, *29*, 1095.
- (2) Penner, S. S. *Energy* **2004**, *31*, 33.
- (3) Nowotny, J.; Sorrell, C. C.; Sheppard, L. R.; Bak, T. *Int. J. Hydrogen Energy* **2005**, *30*, 521.
- (4) Licht, S. *Chem. Commun.* **2005**, *37*, 4635.
- (5) Arakawa, H.; Aresta, M.; Armor, J. N.; Barteau, M. A.; Beckman, E. J.; Bell, A. T.; Bercaw, J. E.; Creutz, C.; Dinjus, E.; Dixon, D. A.; Domen, K.; DuBois, D. L.; Eckert, J.; Fujita, E.; Gibson, D. H.; Goddard, W. A.; Goodman, D. W.; Keller, J.; Kubas, G. J.; Kung, H. H.; Lyons, J. E.; Manzer, L. E.; Marks, T. J.; Morokuma, K.; Nicholas, K. M.; Periana, R.; Que, L.; Rostrup-Nielsen, J.; Sachtler, W. M. H.; Schmidt, L. D.; Sen, A.; Somorjai, G. A.; Stair, P. C.; Stults, B. R.; Tumas, W. *Chem. Rev.* **2001**, *101*, 953.
- (6) Das, D.; Veziroglu, T. N. *Int. J. Hydrogen Energy* **2001**, *26*, 13.
- (7) Irvine, J. J. *Mater. Chem.* **2008**, *18*, 2295.
- (8) York, A. P. E.; Xiao, T.; Green, M. L. H. *Top. Catal.* **2003**, *22*, 345.
- (9) Enger, B. C.; Lodeng, R.; Holmen, A. *Appl. Catal., A* **2008**, *346*, 1.
- (10) Wegang, R. S. *Fuel. Cell Bull.* **2001**, *28*, 8.
- (11) Moghtaderi, B.; Shames, I.; Djenidi, L. *Int. J. Heat Fluid Flow* **2006**, *27*, 1069.
- (12) Moghtaderi, B. *Fuel* **2007**, *86*, 469.
- (13) Pena, M. A.; Gomez, J. P.; Fierro, J. L. G. *Appl. Catal., A* **1996**, *144*, 7.
- (14) Tsang, S. C.; Claridge, J. B.; Green, M. L. H. *Catal. Today* **1995**, *23*, 3.
- (15) Zhu, Q.; Zhao, X.; Deng, Y. *J. Nat. Gas Chem.* **2004**, *13*, 191.
- (16) Liander, H. *Trans. Faraday Soc.* **1929**, *25*, 462.
- (17) Padovani, C.; Franchetti, P. G. *Chim. Ind. Appl. Catal.* **1933**, *15*, 429.
- (18) Prettre, M.; Eichner, C.; Perrin, M. *Trans. Faraday Soc.* **1946**, *42*, 335.
- (19) Brenner, D. W. *Phys. Rev. B* **1990**, *42*, 9458.
- (20) Tersoff, J. *Phys. Rev. B* **1988**, *37*, 6991.
- (21) Johnston, H. S.; Parr, C. J. *Am. Chem. Soc.* **1963**, *85*, 2544.
- (22) Johnston, H. S. *Adv. Chem. Phys.* **1960**, *3*, 131.
- (23) Root, D. M.; Landis, C. M.; Cleveland, T. J. *Am. Chem. Soc.* **1993**, *115*, 4201.
- (24) Cleveland, T.; Landis, C. M. *J. Am. Chem. Soc.* **1996**, *118*, 6020.
- (25) Landis, C. M.; Cleveland, T.; Firman, T. K. *J. Am. Chem. Soc.* **1998**, *120*, 2641.
- (26) Pauling, L. J. *J. Am. Chem. Soc.* **1947**, *69*, 542.
- (27) van Duin, A. C. T.; Dasgupta, S.; Lorant, F.; Goddard, W. A., III. *J. Phys. Chem. A* **2001**, *105*, 9396.
- (28) Chenoweth, K.; van Duin, A. C. T.; Goddard, W. A., III. *J. Phys. Chem. A* **2008**, *112*, 1040.
- (29) Strachan, A.; van Duin, A. C. T.; Chakraborty, D.; Dasgupta, S.; Goddard, W. A., III. *Phys. Rev. Lett.* **2003**, *91*, 098301.
- (30) Zhang, Q.; Cagin, T.; van Duin, A. C. T.; Goddard, W. A., III; Qi, Y.; Hector, L. G. *Phys. Rev. Lett.* **2004**, *69*, 045423.
- (31) van Duin, A. C. T.; Strachan, A.; Stewman, S.; Zhang, Q.; Xu, X.; Goddard, W. A., III. *J. Phys. Chem. A* **2003**, *17*, 3803.
- (32) Chenoweth, K.; Cheung, S.; van Duin, A. C. T.; Goddard, W. A., III; Kober, E. M. *J. Am. Chem. Soc.* **2005**, *127*, 7192.
- (33) Ludwig, J.; Vlachos, D. G.; van Duin, A. C. T.; Goddard, W. A., III. *J. Phys. Chem. B* **2006**, *110*, 4274.
- (34) Nielsen, K. D.; van Duin, A. C. T.; Oxgaard, J.; Deng, W.-Q.; Goddard, W. A., III. *J. Phys. Chem. A* **2005**, *109*, 493.
- (35) Goddard, W. A., III; Merinov, B.; van Duin, A. C. T.; Jacob, T.; Blanco, M.; Molinero, V.; Jang, S. S.; Jang, Y. H. *Mol. Simul.* **2006**, *32*, 251.
- (36) Berendsen, H. J. C.; Postma, J. P. M.; van Gunsteren, W. F.; DiNola, A.; Haak, J. R. *J. Phys. Chem. B* **1984**, *81*, 3684.
- (37) Becke, A. D. *J. Chem. Phys.* **1993**, *98*, 5648.
- (38) Lee, C.; Yang, W.; Parr, R. G. *Phys. Rev. B* **1998**, *37*, 785.
- (39) Krishnan, R.; Binkley, J. S.; Seeger, R.; Pople, J. A. *J. Chem. Phys.* **1980**, *72*, 650.
- (40) Merrick, J. P.; Moran, D.; Radom, L. *J. Phys. Chem. A* **2007**, *111*, 11683.
- (41) Martin, J. M. L.; de Oliveira, G. *J. Chem. Phys.* **1999**, *111*, 1843.
- (42) Frisch, M. J.; Trucks, G. W.; Schlegel, H. B.; Scuseria, G. E.; Robb, M. A.; Cheeseman, J. R.; Montgomery, J. A., Jr.; Vreven, T.; Kudin, K. N.; Burant, J. C.; Millam, J. M.; Iyengar, S. S.; Tomasi, J.; Barone, V.; Mennucci, B.; Cossi, M.; Scalmani, G.; Rega, N.; Petersson, G. A.; Nakatsuji, H.; Hada, M.; Ehara, M.; Toyota, K.; Fukuda, R.; Hasegawa, J.;



- Ishida, M.; Nakajima, T.; Honda, Y.; Kitao, O.; Nakai, H.; Klene, M.; Li, X.; Knox, J. E.; Hratchian, H. P.; Cross, J. B.; Bakken, V.; Adamo, C.; Jaramillo, J.; Gomperts, R.; Stratmann, R. E.; Yazyev, O.; Austin, A. J.; Cammi, R.; Pomelli, C.; Ochterski, J. W.; Ayala, P. Y.; Morokuma, K.; Voth, G. A.; Salvador, P.; Dannenberg, J. J.; Zakrzewski, V. G.; Dapprich, S.; Daniels, A. D.; Strain, M. C.; Farkas, O.; Malick, D. K.; Rabuck, A. D.; Raghavachari, K.; Foresman, J. B.; Ortiz, J. V.; Cui, Q.; Baboul, A. G.; Clifford, S.; Cioslowski, J.; Stefanov, B. B.; Liu, G.; Liashenko, A.; Piskorz, P.; Komaromi, I.; Martin, R. L.; Fox, D. J.; Keith, T.; Al-Laham, M. A.; Peng, C. Y.; Nanayakkara, A.; Challacombe, M.; Gill, P. M. W.; Johnson, B.; Chen, W.; Wong, M. W.; Gonzalez, C.; Pople, J. A. *Gaussian 03*, revision E.01; Gaussian, Inc.: Wallingford, CT, 2004.
- (43) Stanton, J. F.; Gauss, J.; Watts, J. D.; Lauderdale, W. J.; Bartlett, R. J. *Int. J. Quant. Chem. Symp.* **1992**, 26, 879.
- (44) Srinivasan, N. K.; Micheal, J. V.; Harding, L. B.; Klippenstein, S. J. *Combust. Flame* **2007**, 149, 104.
- (45) Zhu, R.; Hsu, C.-C.; Lin, M. C. *J. Chem. Phys.* **2001**, 115, 195.
- (46) Petersen, E. L.; Davidson, D. F.; Hanson, R. K. *J. Propul. Power* **1999**, 15, 8291.
- (47) Petersen, E. L.; Kalitan, D. M.; Simmons, S.; Bourque, G.; Curran, H. J.; Simmie, J. M. *Proc. Combust. Inst.* **2007**, 31, 447454.
- (48) Simmie, J. M. *Prog. Energy Combust. Sci.* **2003**, 29, 599.
- (49) Taatjes, C. A.; Meloni, G.; Selby, T. M.; Trevitt, A. J.; Osborn, D. L.; Percival, C. J.; Shallcross, D. E. *J. Am. Chem. Soc.* **2008**, 130, 11883.
- (50) Andersen, A.; Carter, E. A. *J. Phys. Chem. A* **2003**, 107, 9463.
- (51) Chen, B.-Z.; Anglada, J. M.; Huang, M.-B.; Kong, F. *J. Phys. Chem. A* **2002**, 106, 1877.
- (52) Fang, D.-C.; Fu, X.-Y. *J. Phys. Chem. A* **2002**, 106, 2988.
- (53) Alvarez, R. A.; Moore, C. B. *J. Phys. Chem.* **1994**, 98, 174.
- (54) Huang, M.-B.; Chen, B.-Z.; Wang, Z.-X. *J. Phys. Chem. A* **2002**, 106, 5490.
- (55) Clark, T.; Chandrasekhar, J.; Spitznagel, G. W.; von Rague-Schleyer, P. *J. Comput. Chem.* **1983**, 4, 294.
- (56) Frisch, M. J.; Pople, J. A.; Binkley, J. S. *J. Chem. Phys.* **1984**, 80, 3265.
- (57) Woon, D. E.; Dunning, T. H. *J. Phys. Chem.* **1993**, 98, 1358.
- (58) Chase, M. W., Jr. *NIST-JANAF Thermochemical Tables*, 4th ed.; American Chemical Society: Washington, DC, 1998.
- (59) Curtiss, L. A.; Raghavachari, K.; Trucks, G. W.; Pople, J. A. *J. Chem. Phys.* **1991**, 94, 7221.
- (60) Slagle, I. R.; Gutman, D. *J. Am. Chem. Soc.* **1985**, 107, 5432.

JP809576K